EXPERIMENTAL AND NUMERICAL COMPARISON OF TRANSITION FOR LOW-REYNOLDS NUMBER AIRFOILS

Paul Ziadé

Department of Mechanical and Industrial Engineering
University of Toronto
5 King's College Rd., Toronto, Ontario, M5S 3G8, Canada
paul.ziade@mail.utoronto.ca

Pierre E. Sullivan

Department of Mechanical and Industrial Engineering
University of Toronto
5 King's College Rd., Toronto, Ontario, M5S 3G8, Canada
sullivan@mie.utoronto.ca

ABSTRACT

A numerical and experimental study of a NACA 0025 airfoil at a Reynolds number of 10^5 and two angles of attack (5° and 12°) is conducted. In this investigation, large-eddy simulation is employed to compute the separation, transition, and reattachment behaviour of the shear layer. Good agreement between the numerics and experiment is found. A laminar separation bubble is formed at an angle of attack of 5° whereas no reattachment occurs at the larger angle of attack. Receptivity effects are likely the cause of a slightly overpredicted laminar separation bubble length, as these are not accounted for in the computations. Linear stability analysis is performed on the base velocity profiles obtained from the computations and experiment. Despite excellent boundary layer profile agreement, it is found that fairly large differences in the growth rate spectra are obtained. A sensitivity analysis using a matrix perturbation technique is discussed and shows that the Orr-Sommerfeld operator, which governs the stability behaviour, is highly sensitive to base flow perturbations. This acute sensitivity makes direct comparisons of stability behaviour a challenge, and this sensitivity should be taken into account.

INTRODUCTION

Unmanned aerial vehicles (UAVs), small-scale wind turbines, and low-speed aircraft operate in the low Reynolds number regime, $Re_c < 500{,}000$ (DeLaurier (2003)), where Re_c is the chord-based Reynolds number. Unlike high Reynolds number flow, the laminar boundary layer often separates due to a strong adverse pressure gradient. The separated flow can transition to turbulence and potentially reattach to the airfoil surface thus forming a laminar separation bubble (LSB) (Tani (1964)).

High-fidelity computational methods, *e.g.*, large-eddy simulation (LES), provide a much more detailed view of the separation and transition events. LES also enables computation of aerodynamic noise (Kim *et al.* (2006)) and can inform flow control strategies (You *et al.* (2008)). LES has also seen success with low-Reynolds number airfoils (Eisenbach & Friedrich (2008); Kojima *et al.* (2003)) and in the prediction of stall behaviour and laminar separation bubbles (Alferez *et al.* (2013); Mary & Sagaut (2002)). The higher resolution obtained by LES can be advantageous for linear stability studies, as the resulting eigenvalue spectra have been shown to be very sensitive to experimental data scatter (Boutilier & Yarusevych (2013)).

The sensitivity of one-dimensional linear stability analysis has been reported in several papers (Bottaro *et al.* (2003)). Large deviations in the eigenvalue spectrum representing the growth rate have been attributed to the non-normality of the linear stability operator (Reddy *et al.* (1993)), because the non-normal matrix is one which does not commute with its adjoint, $AA^\star \neq A^\star A$. These matrices, therefore, have nonorthogonal eigenfunctions. The analysis of these types of operators has been performed using matrix perturbation techniques such as the ε-pseudospectrum.

The present investigation is a numerical and experimental study of a NACA 0025 airfoil at a Reynolds number of 10^5; well within the low Reynolds number regime. Numerical simulations are employed to investigate the transient shear layer at two angles of attack; $AOA \in [5^\circ, 12^\circ]$. Of particular interest were boundary layer separation, existence of laminar separation bubble, and stability and transition. Linear stability analysis was performed on the separated shear layer profiles obtained from LES and experiment. The linear stability analysis is complemented with a sensitivity analysis of the stability equations.

METHODOLOGY

The computational procedure for the LES investigation is described. In addition, the Chebyshev collocation method for the solution of the stability equations is discussed.

Numerical Methodology

The numerical computations were performed by solving the filtered Navier-Stokes equations for large-eddy simulation. For incompressible flow, the governing equations are:

$$\frac{\partial \overline{u_i}}{\partial x_i} = 0 \tag{1}$$

$$\frac{\partial \overline{u_i}}{\partial t} + \frac{\partial}{\partial x_j}(\overline{u_i}\,\overline{u_j}) = -\frac{\partial \overline{p}}{\partial x_i} + \nu \frac{\partial}{\partial x_j}\left(\frac{\partial \overline{u_i}}{\partial x_j} + \frac{\partial \overline{u_j}}{\partial x_i}\right) - \frac{\partial \tau_{ij}}{\partial x_j}, \tag{2}$$

where $\overline{f}$ denotes a filtered variable. The SGS stress tensor, τ_{ij}, is closed using an eddy viscosity approach, $\tau_{ij} = -2\nu_r \overline{S}_{ij}$, where ν_r is

the eddy viscosity. A subgrid-scale turbulence kinetic energy model was employed, where $k = \frac{1}{2}\sum_i(\tau_{ii})$ is the SGS kinetic energy, whose transport equation is

$$\frac{\partial k}{\partial t} + \frac{\partial}{\partial x_i}(k\overline{u_i}) = \frac{\partial}{\partial x_i}\left[(\nu + \nu_r)\frac{\partial k}{\partial x_i}\right] - \varepsilon - \tau_{ij}S_{ij}. \quad (3)$$

The eddy viscosity and dissipation rate, ε, are evaluated as follows to close the system:

$$\nu_r = C_k k^{1/2}\Delta \quad \varepsilon = C_\varepsilon k^{3/2}/\Delta, \quad (4)$$

where $C_\varepsilon = 1.048$ and $C_k = 0.094$.

The temporal and convective terms were discretized using a second order backward implicit time stepping scheme and second order TVD scheme, respectively. An adaptive time stepping scheme was employed to maintain a CFL number of $Co < 0.7$ throughout the domain. The PISO algorithm was used for the pressure-momentum coupling. The airfoil surface was defined as a no-slip boundary condition and a periodic boundary condition was applied to the lateral boundaries, spaced $c/2$ apart, where c is the chord length. The inlet and outlet were assigned laminar inflow and zero-gradient outflow conditions, respectively.

The computations were performed on 64-128 processors using the Blue Gene/Q (BGQ) and General Purpose Cluster (GPC) at Scinet (Loken *et al.* (2010)). Approximately 7 hours were required to compute one convective time-scale, $t_{conv} = c/U_\infty$. Statistics were observed for $33t_{conv}$. Statistics of the flow started being computed at approximately $t = 17t_{conv}$ for all cases considered. A block-structured C-mesh with 32×10^6 cells was employed with mesh refinement concentrated in the wake and around the NACA 0025 airfoil with chord length $c = 0.3m$. For wall-resolved LES, it is well accepted that the required mesh resolution, which has been achieved in all cases (Fig. 1), is $\Delta x^+ \approx 100$, $\Delta y^+ \approx 2$, and $\Delta z^+ \approx 20$ (Sagaut (2006); Mary& Sagaut (2002)). In addition to the global $x-y$ coordinate system, some results are presented with respect to a local $x'-y'$ coordinate system, with the origin at the leading edge, x' aligned with the chord and increasing toward the trailing edge, and y' aligned with the local wall-normal direction on the airfoil suction side. Another measure of the quality and resolution of the simulations is the resolved-to-turbulent kinetic energy ratio, γ:

$$\gamma = \frac{k_{res}}{k_{SGS} + k_{res}} \quad (5)$$

where k_{res} is the turbulent kinetic energy in the resolved scales, and k_{SGS} is the the subgrid-scale kinetic energy. A well-resolved LES should resolve at least 80% of the turbulent kinetic energy, according to Pope (2004). Figure 2 shows the kinetic energy ratio at several locations.

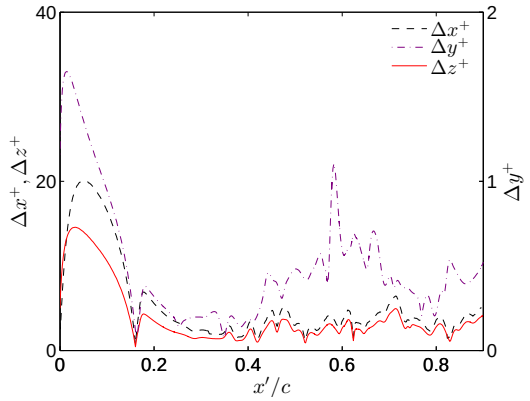

Figure 1: The near-wall mesh spacing for the NACA 0025 at $AOA = 10^\circ$.

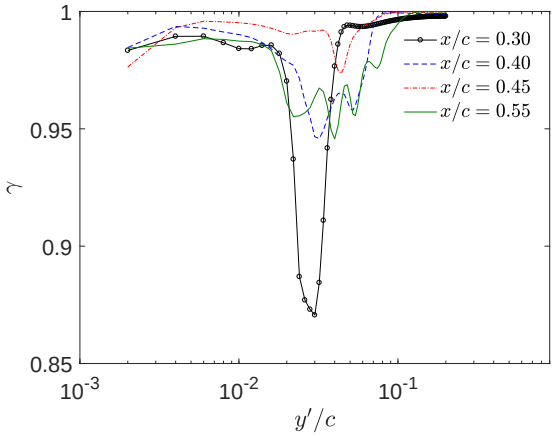

Figure 2: Kinetic energy ratio, γ, at several locations. $AOA = 10^\circ$.

Linear Stability Analysis

Linear stability analysis (LSA) was performed on the velocity profiles from LES and hot-wire experiments. Small velocity and pressure perturbations are considered, where

$$\boldsymbol{v}(\boldsymbol{x_i},t) = \boldsymbol{V}(y) + \boldsymbol{v'}(\boldsymbol{x_i},t), \quad p(\boldsymbol{x_i},t) = P + p'(\boldsymbol{x_i},t). \quad (6)$$

The stability of the mean base flow is assessed by its response to wavelike perturbations expressed as,

$$v'(x_i,t) = \tilde{v}(y)e^{i(\alpha x - \omega t)} \quad (7)$$

where $\alpha = \alpha_r + i\alpha_i$ is the complex wavenumber and ω is the real frequency. Formulations in which the wavenumber is complex correspond to the spatial stability problem, where the solution can grow or decay in space and only oscillate in time at a particular location. By substituting the above decomposition and normal mode wavelike perturbation in the Navier-Stokes equations, the Orr-Sommerfeld Equation is obtained:

$$\left(U - \frac{\omega}{\alpha}\right)\left(\frac{d^2\tilde{v}}{dy^2} - \alpha^2\tilde{v}\right) - \frac{d^2U}{dy^2}\tilde{v} = -\frac{i}{\alpha Re}\left(\frac{d^4\tilde{v}}{dy^4} - 2\alpha^2\frac{d^2\tilde{v}}{dy^2} + \alpha^4\tilde{v}\right). \quad (8)$$

The growth rate of the perturbations is determined by eigenvalues with $-\alpha_i$.

This study employed a Chebyshev collocation approach for the solution of Eqn. 8. The semi-infinite domain of the shear layer profile, $y \in [0,\infty)$, was mapped onto the domain $\eta \in [-1,1]$ by using an algebraic mapping function, $f(\eta)$. Algebraic mappings have been reported as superior to logarithmic mappings by Boyd (2001) and Schmid and Henningson (2001).

The n^{th} Chebyshev polynomial of the first kind is

$$T_n(\eta) = \cos(n\cos^{-1}\eta). \tag{9}$$

The transformed equations are solved at the Gauss-Lobatto points. The vertical velocity fluctuation in (8) is expressed as a Chebyshev polynomial series,

$$\tilde{v}(\eta) = \sum_{n=1}^{N} a_n T_n(\eta) \tag{10}$$

with boundary conditions in Chebyshev space (Schmid and Henningson (2001)),

$$\begin{aligned} \sum_{n=1}^{N} a_n T_n(1) = 0; \quad \sum_{n=1}^{N} a_n T_n(-1) = 0 \\ \sum_{n=1}^{N} a_n T_n'(1) = 0; \quad \sum_{n=1}^{N} a_n T_n'(-1) = 0. \end{aligned} \tag{11}$$

Substituting the above Chebyshev expansions into the Orr-Sommerfeld equation yields a polynomial eigenvalue problem with matrix coefficients, C_j (Bridges (1984); Liou (1992)). For the Orr-Sommerfeld equation, a fourth order polynomial with α as the complex parameter is obtained (Bridges (1984)):

$$\boldsymbol{D_4}(\alpha)\boldsymbol{a} = 0 \tag{12}$$

where,

$$\boldsymbol{D_4}(\alpha) = \boldsymbol{C_0}\alpha^4 + \boldsymbol{C_1}\alpha^3 + \boldsymbol{C_2}\alpha^2 + \boldsymbol{C_3}\alpha + \boldsymbol{C_4}. \tag{13}$$

The polynomial eigenvalue problem can be reformulated using the companion matrix method to yield a complex generalized eigenvalue problem:

$$\left(\begin{bmatrix} -C_1 & -C_2 & -C_3 & -C_4 \\ I & 0 & 0 & 0 \\ 0 & I & 0 & 0 \\ 0 & 0 & I & 0 \end{bmatrix} - \alpha \begin{bmatrix} C_0 & 0 & 0 & 0 \\ 0 & I & 0 & 0 \\ 0 & 0 & I & 0 \\ 0 & 0 & 0 & I \end{bmatrix} \right) \begin{Bmatrix} \alpha^3\boldsymbol{a} \\ \alpha^2\boldsymbol{a} \\ \alpha\boldsymbol{a} \\ \boldsymbol{a} \end{Bmatrix} = 0.$$

The above approach was used to solve the viscous spatial stability problem defined by the Orr-Sommerfeld equation.

RESULTS

The following describe the numerical and experimental results. A detailed comparison is presented in Ziadé *et al.* (2017).

Flow Features

Instantaneous flow field results are visualized using the Q-criterion. The shear layer and wake structure for the two angles of attack considered, $AOA \in [5^o, 12^o]$, is presented in Fig. 3a and Fig. 3b.

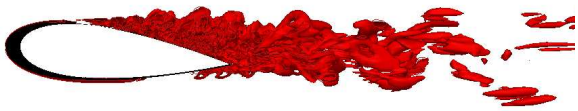

(a)

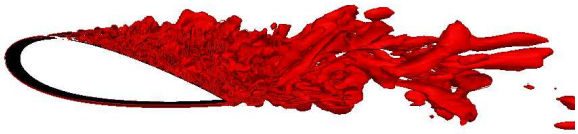

(b)

Figure 3: $Q = 2500$ contours - a) $AOA = 5°$, b) $AOA = 12°$,

Flow separation occurs shortly downstream of the leading edge for the two angles of attack considered. A wide range of scales is observed, with larger structures identified at the higher angle of attack. The extent of the wake increases with increasing angle of attack. An isometric view of the airfoil at $AOA = 5°$ is shown in figure 4 which shows a vortex roll-up which rapidly breaks down to three-dimensional turbulence. This initial vortex is largely two-dimensional, spans the width of the airfoil, and is due to a two-dimensional Tollmien-Schlichting wave. Before final breakdown, hairpin structures are also observed in the transitional region.

Figure 4: Isosurface of $Q = 2500\,s^{-2}$ at $AOA = 5°$.

Laminar Separation Bubble

The mean surface pressure distribution on the airfoil suction surface can help determine the separation point. As Carmichael notes (Carmichael 1981), a boundary layer that fails to reattach displays a nearly constant static pressure extending from the separation point to the trailing edge. On the other hand, a rapid pressure recovery indicates that the flow has transitioned and reattached to the air-

foil, leading to a laminar separation bubble. The coefficient of pressure, $C_p = (p - p_\infty)/(0.5\rho U_\infty^2)$, is presented figure 5. Both angles

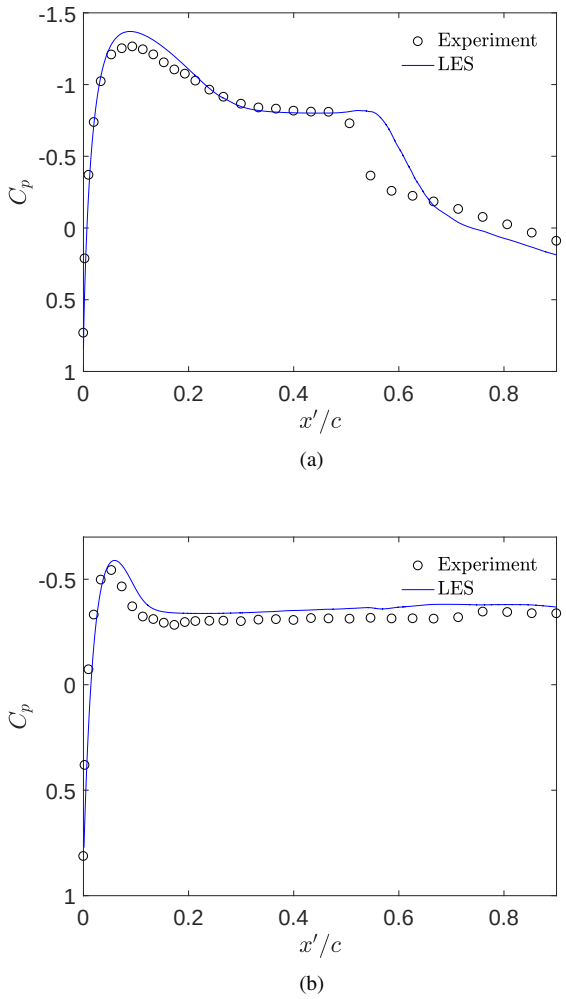

Figure 5: Pressure Coefficient - a) $AOA = 5^\circ$, b) $AOA = 12^\circ$.

of attack considered exhibit the constant C_p typical of a separated boundary layer. $AOA = 12^\circ$ displays a constant C_p region which extends from the separation point to the trailing edge suggesting no boundary layer reattachment. On the other hand, $AOA = 5^\circ$ has a constant pressure region followed by a sudden pressure recovery. This suggests the presence of a laminar separation bubble. As well, the separation point moves forward with increasing angle of attack. As can be seen from the pressure coefficient plots, there is good agreement between the experiment and computations. The laminar separation bubble is slightly overpredicted. One possible source of this variance is receptivity, which often cannot be accounted for in experiments and can greatly affect the behaviour of low-Reynolds number airfoils (Dovgal and Kozlov (1983)).

The shear layer separation and laminar separation bubble can better be visualized by the mean velocity streamlines (figure 6). At the higher angle of attack in figure 6b, a low velocity recirculating region is observed over a good portion of the airfoil upper surface. This low velocity region extends well beyond the trailing edge, once again suggesting no reattachment. This is not the case, however, for $AOA = 5^\circ$ (figure 6a) as only a small low-velocity region, the laminar separation bubble, is seen near the surface followed by a recovery.

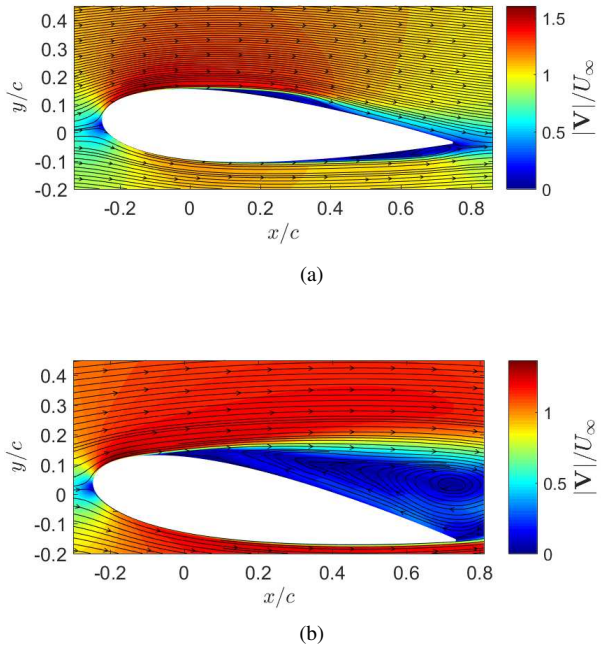

Figure 6: Mean LES velocity streamlines - a) $AOA = 5^\circ$, b) $AOA = 12^\circ$.

Stability Analysis

Mean velocity profiles obtained from the numerical computations and hot-wire measurements were used in the stability computations. A hyperbolic tangent fit (Dovgal (1994)) was applied to the velocity data using a least-squares method (eqn. 14), as suggested by Boutilier and Yarusevych (2013) who found that analytical expressions provide more reliable predictions for linear stability analysis.

$$\frac{U(y')}{U_e} = \frac{\tanh[a_1(y'-a_2)] + \tanh(a_1 a_2)}{1 + \tanh(a_1 a_2)} + a_3 \frac{y'}{a_2} \exp\left[-1.5\left(\frac{y'}{a_2}\right)^2 + 0.5\right] \tag{14}$$

where a_1, a_2 and a_3 are the fit parameters and U_e is the edge velocity.

The wall-normal profiles of the mean velocity, U, just downstream of separation are shown in figure 7. The hyperbolic tangent curve fit provides a good analytical approximation to the discrete data. The maximum normalized least squares residual for the boundary layers is $R = 0.001$.

Using the analytical boundary layer curve fits, unstable frequency-growth rate profiles were generated using linear stability analysis (figure 8). In addition, experimentally-measured growth rates were determined from hot-wire measurements at $y' = \delta^\star$. A few trends are of note. The band of unstable frequencies is larger for $AOA = 5^\circ$ than $AOA = 12^\circ$. This is predicted using both the LSA from the LES and experimental profiles. On the other hand,

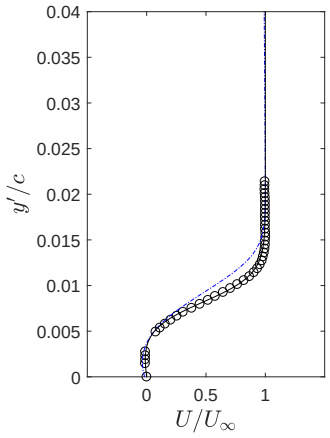

(a)

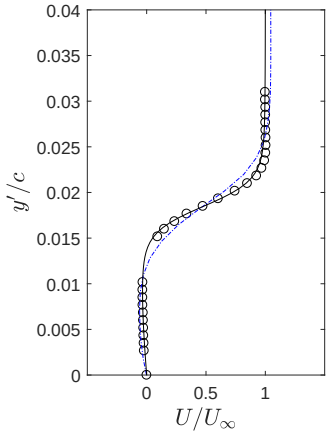

(b)

Figure 7: Boundary Layer Profiles - a) $AOA = 5°$, b) $AOA = 12°$. ○ : Experiment, —— : Analytical curvefit, -·-·-·- : LES.

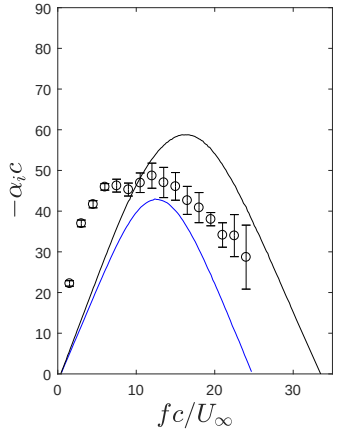

(a)

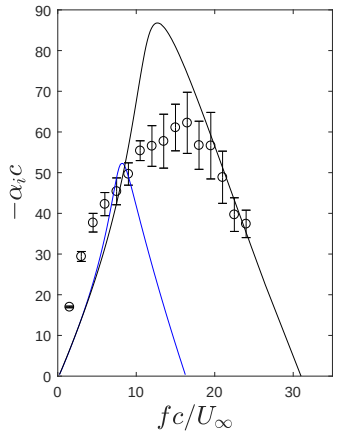

(b)

Figure 8: Unstable stability profiles - a) $AOA = 5°$, b) $AOA = 12°$. ○ : Experiment, —— : Experimental LSA, —— : LES LSA.

peak growth rates, both from LSA predictions and hot-wire measurements, are higher for $AOA = 12°$ compared to $AOA = 5°$.

It is evident, however, that there is some variance between the LSA predictions for LES and experimental velocity profiles. A few studies have investigated the sensitivity of the Orr-Sommerfeld operator (Reddy (1993); Bottaro (2003)). Using the method described in Bottaro (2003) and more recently in Ziadé and Sullivan (2017), the sensitivity of the linear stability predictions can be assessed. In perturbing the base flow, U, with normally distributed noise, the methodology can be considered as a special case of the ε-pseudospectra method (Trefethen (2005)). This alternate method is the ΔU-pseudospectrum, where only the base flow is perturbed. The ΔU-pseudospectrum of a matrix A is defined as

$$\sigma_{\Delta U}(A) = \{z \in \mathbb{C} : z \in \sigma[A(U+\Delta U)] \text{ for some } \Delta U \text{ with } \|\Delta U\| \leq r\}. \quad (15)$$

In the study by Ziadé and Sullivan (2017), the boundary layer profile over a low Reynolds number airfoil was subjected to different levels of perturbation at different Reynolds numbers in the low Reynolds number regime. In figure 9, the growth rate spectra for the perturbed boundary layer at $AOA = 5°$ and $Re_c = 10^5$ is shown. Three levels of velocity perturbations are considered: $\sigma_U = 0.75\%, 1.25\%$, and 2.5%, where σ_U denotes the standard deviation of the imposed normal velocity scatter.

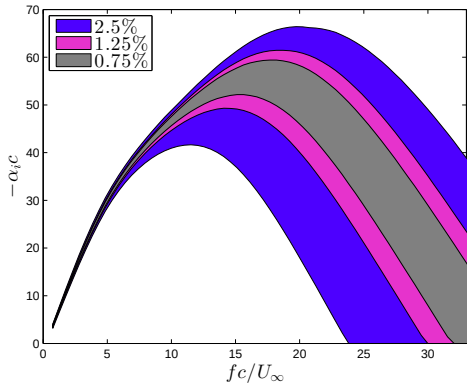

Figure 9: Growth rate spectra with imposed velocity perturbations - $AOA = 5°$.

It is found that even relatively small scatter in the data can produce significant deviations in predicted growth rates and frequencies. As stated earlier, several researchers have attributed this amplified sensitivity, which can be much greater than the perturbation, to the nonnormality of the Orr-Sommerfeld operator (Schmid

et al.(1993), Reddy *et al.* (1993)). Placing this sensitivity study in context, figure 10 shows the growth rate spectra for the perturbed $AOA = 5^\circ$ experimental boundary layer profile plotted with the LES LSA growth rate as well as the measured growth rate.

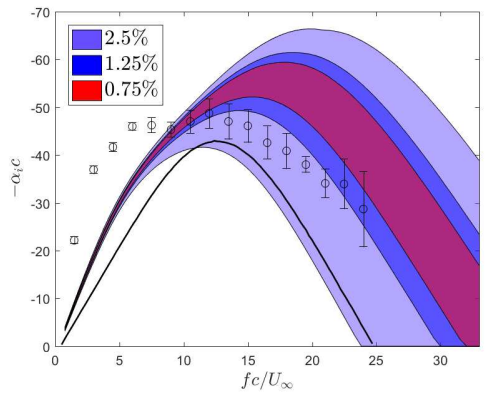

Figure 10: Perturbed growth rates as well as LES growth rate (——) and experimental growth rate (○) - $AOA = 5^\circ$.

It can be seen in figure 10 that the LSA growth rate obtained from the LES velocity profile draws nearer to the nominal growth rate from the experimental velocity profile (figure 8a) if typical velocity scatter is considered. The acute sensitivity of the Orr-Sommerfeld equation, therefore, makes comparison of growth rate spectra using boundary layer profiles from different sources a very difficult task. One should therefore keep this sensitivity in mind when comparing linear stability predictions.

CONCLUSIONS

This study investigated the flow separation and transition over a NACA 0025 airfoil at a Reynolds number of 10^5 at two angles of attack: 5° and 12°. Numerical computations using large-eddy simulation were compared to hot-wire measurements obtained in a low-turbulence wind tunnel.

Pressure measurements on the suction surface of the airfoil agreed well and predicted a laminar separation bubble at $AOA = 5^\circ$ and no reattachment at $AOA = 12^\circ$. The laminar separation bubble was slightly overpredicted in the computations. This variance can likely be attributed to receptivity.

Boundary layer profiles showed very good agreement between experiment and computations. Linear stability analysis was performed on the base profiles using a Chebychev collocation method. The resulting growth rate spectra predicted a wider band of unstable frequencies for $AOA = 5^\circ$ but higher growth rates at $AOA = 12^\circ$.

Fairly pronounced differences were found in the linear stability predictions. It was shown using a matrix perturbation method that the Orr-Sommerfeld operator is very sensitive to base flow perturbations. Accounting for these perturbations, which represent typical experimental velocity scatter, can guide future stability comparisons and provide an explanation for observed growth rate differences despite similar base velocity profiles.

REFERENCES

Alferez, N., *et al.*, 2013, "Study of stall development around an airfoil by means of high fidelity large eddy simulation", *Flow, Turbulence and Combustion*, **91**(3), 623-641.

Bottaro, A., *et al.*, 2003, "The effect of base flow variation on flow stability", *Journal of Fluid Mechanics*, **476**, 293-302.

Boutilier, M., and Yarusevych, S., 2013, "Sensitivity of linear stability analysis of measured separated shear layers", *European Journal of Mechanics, B/Fluids*, **37**, 129-142.

Boyd, J.P., 2001, "Chebyshev & Fourier Spectral Methods", *Dover*.

Bridges, T.J., and Morris, P.J., 1984, "Differential eigenvalue problems in which the parameter appears nonlinearly", *Journal of Computational Physics*, **55**, 437-460.

Carmichael, B.H., 1981, "Low Reynolds number airfoil survey, Volume I", NASA Contractor Report 165803.

Dovgal, A.V., and Kozlov, V.V., 1983, "Influence of acoustic perturbations on the flow structure in a boundary layer with adverse pressure gradient," *Fluid Dynamics*, **18**, 205-209.

Dovgal, A.V., *et al.*, 1994, "Laminar boundary layer separation: Instability and associated phenomena", *Progress in Aerospace Sciences*, **30**(1), 61-94.

Eisenbach, S., and Friedrich, R., 2008, "Large-eddy simulation of flow separation on an airfoil at a high angle of attack and Re=10^5 using Cartesian grids", *Theoretical and Computational Fluid Dynamics*, **22**(3-4), 213-225.

Kim, H.J. *et al.*, 2006, "Computation of unsteady flow and aerodynamics noise of NACA 0018 airfoil using large-eddy simulation", *International Journal of Heat and Fluid Flow*, **27**(2), 229-242.

Kojima, R., *et al.*, 2013, "Large-eddy simulation of low-Reynolds-number flow over thick and thin NACA airfoils", *Journal of Aircraft*, **50**(1), 187-196.

Liou, W.W., and Morris, P.J., 1991, "A comparison of numerical methods for the Rayleigh equation in unbounded domains", NASA Technical Memorandum 105179.

Loken, C., *et al.*, 2010, "SciNet: Lessons learned from building a power-efficient top-20 system and data centre", *Journal of Physics: Conference Series*, **256**(1).

Mary, I., and Sagaut, P., 2002, "Large eddy simulation of flow around an airfoil near stall", *AIAA Journal*, **40**(6), 1139-1145.

Mueller, T.J., and DeLaurier, J.D., 2003, "Aerodynamics of Small Vehicles",*Annual Review of Fluid Mechanics*, **35**, 89-111.

Pope, S., 2004, "Ten questions concerning the large-eddy simulation of turbulent flows", *New Journal of Physics*, **6**(35).

Reddy, S.C., *et al.*, 1993, "Pseudospectra of the Orr-Sommerfeld operator", *SIAM Journal of Applied Mathematics*, **53**(1), 15-47.

Sagaut, P., 2006, "Large eddy simulation for incompressible flows", *Springer*.

Schmid, P.J., *et al.*, 1993, "A study of eigenvalue sensitivity for hydrodynamic stability operators", *Theoretical and Computational Fluid Dynamics*, **4**, 227-240.

Schmid, P.J., and Henningson, D.S., 2001, "Stability and Transition in Shear Flows", *Applied Mathematical Sciences***142**, Springer.

Tani, I., 1964, "Low-Speed Flows Involving Bubble Separations", *Progress in Aerospace Sciences*, **5**, 70-103.

Trefethen, L.N., and Embree, M., 2005, "Spectra and Pseudospectra", Princeton University Press.

You, D. *et al.*, 2008, "Discrete conservation principles in large-eddy simulation with application to separation control over an airfoil", *Physics of Fluids*, **20**(10), 101515.

Ziadé, P., *et al.*, 2017, "Shear layer development, separation, and stability over a low-Reynolds number airfoil", In Preparation.

Ziadé, P., and Sullivan, P.E., 2017, "Sensitivity of the Orr-Sommerfeld equation to base flow perturbations with application to airfoils", Submitted to *International Journal of Heat and Fluid Flow.*